Supplementary Material for

Cyano-modified poly(triazine imide) with extended π-conjugation for photocatalytic biological cofactor regeneration

Jianhua Liu,[a,b] *Jiashu Li,*[a,b] *Fangshu Xing*[b,] * *and Jian Liu*[a, b,] *

[a] College of Materials Science and Engineering, Qingdao University of Science and Technology, Qingdao 266042, P. R. China

[b] Qingdao Institute of Bioenergy and Bioprocess Technology, Chinese Academy of Sciences, Shandong Energy Institute, Qingdao New Energy Shandong Laboratory, Qingdao 266101, P. R. China

*Corresponding authors.

E-mail addresses: xingfs@qibebt.ac.cn; liujian@qibebt.ac.cn

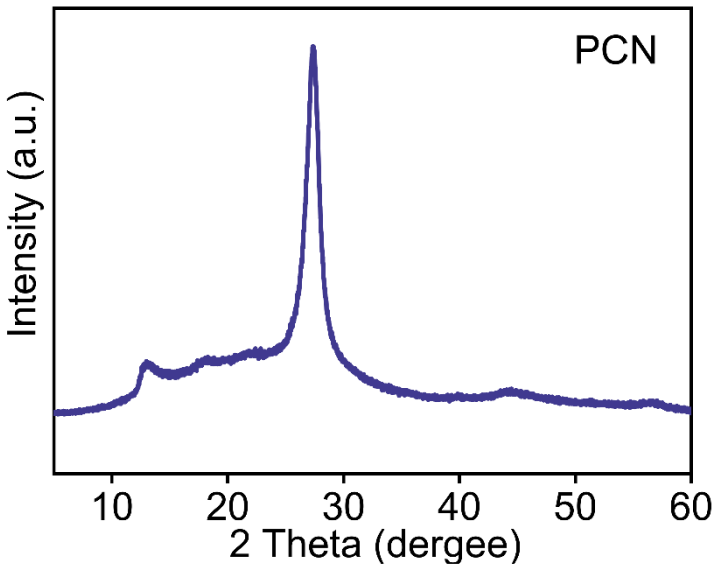

Fig. S1. XRD pattern of PCN.

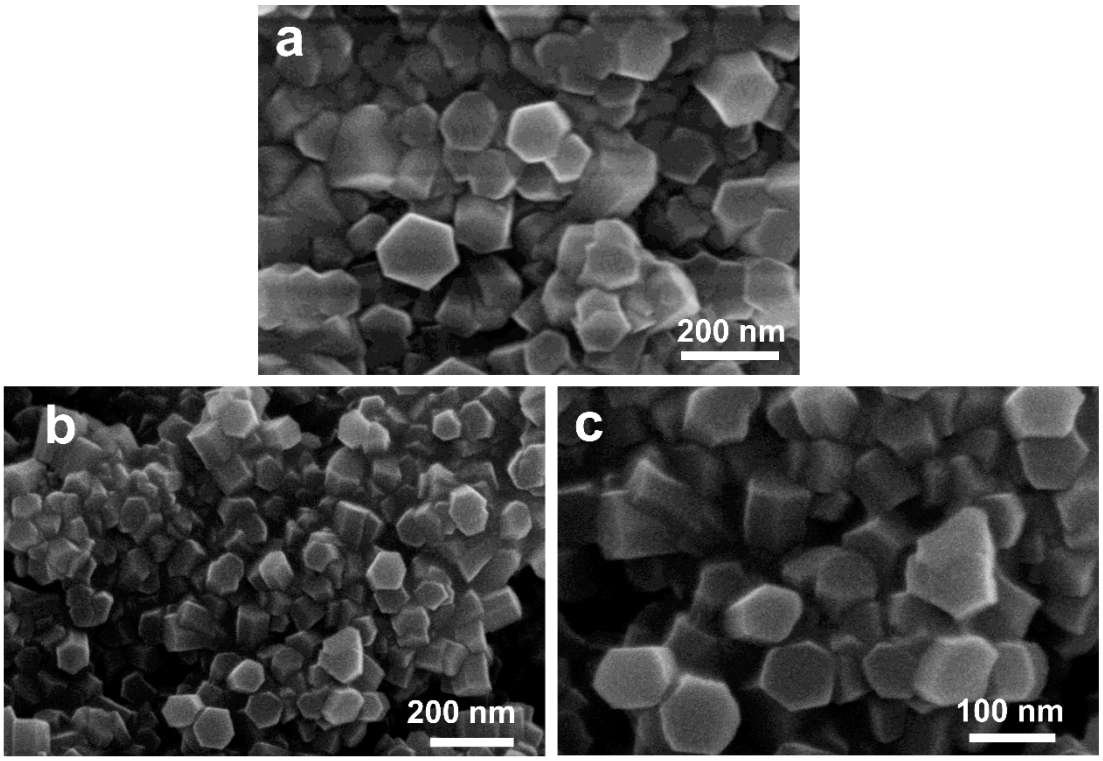

Fig. S2. (a) SEM images of PTI and (b, c) D-PTI-350 samples.

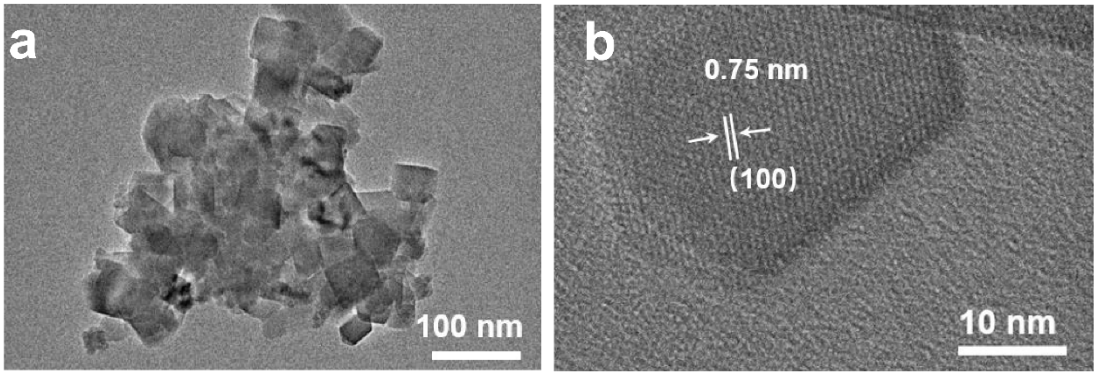

Fig. S3. (a) TEM and (b) HRTEM images of PTI.

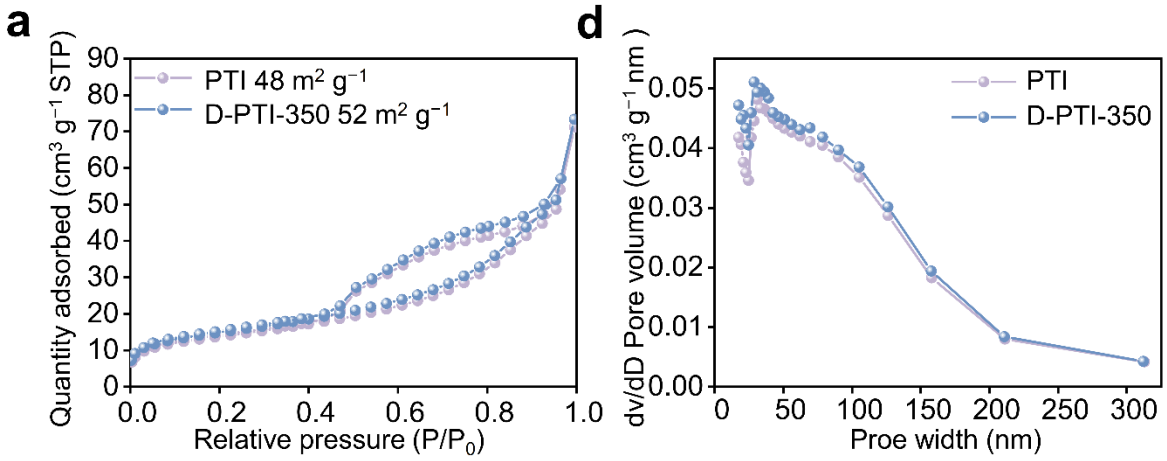

Fig. S4. (a) N_2 adsorption–desorption isotherms and (b) corresponding pore size distribution curves of PTI and D-PTI-350, respectively.

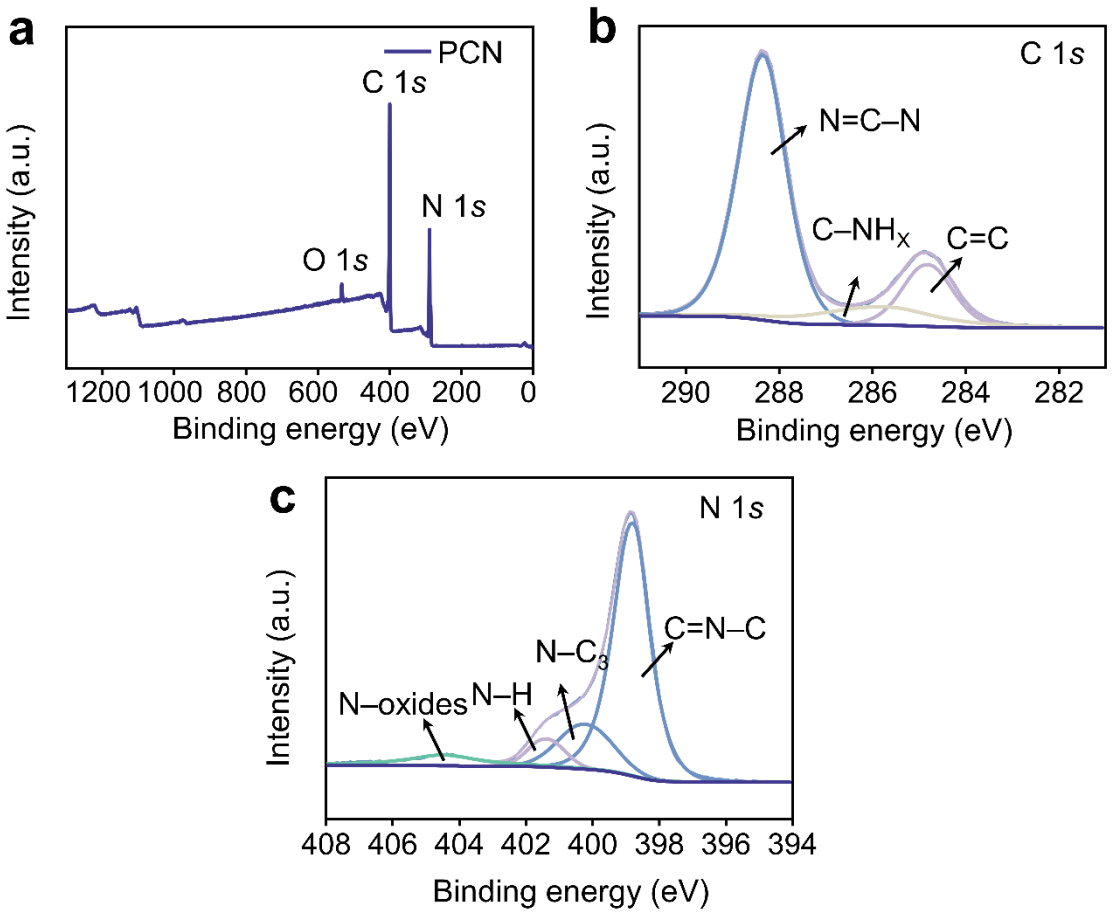

Fig. S5. (a) Survey XPS spectra, (b) C 1*s*, and (c) N 1*s* high-resolution spectra of as-prepared PCN.

The PCN sample was composed of two elements: C and N. The C 1*s* spectrum in the PCN sample can be deconvoluted into three peaks located at binding energy of 288.2, 286.3 and 284.8 eV, which are attributed to the C in the aromatic N–C=N moiety, the C in the C-NH_x (x = 1 or 2) moieties at the edges of the tri-s-triazine units and the C in the amorphous carbon and aromatic C=C bonds used as calibration standards, respectively.[1] In the N 1*s* spectrum, the fitted peaks at 398.8, 399.5, 401.0 and 404.3 eV correspond to the pyridinic N in the tri-s-triazine units, graphitic N, N-H species and π–π* excitations in conjugated aromatic rings, respectively.[2] These results are consistent with the typical XPS characteristics of PCN samples.

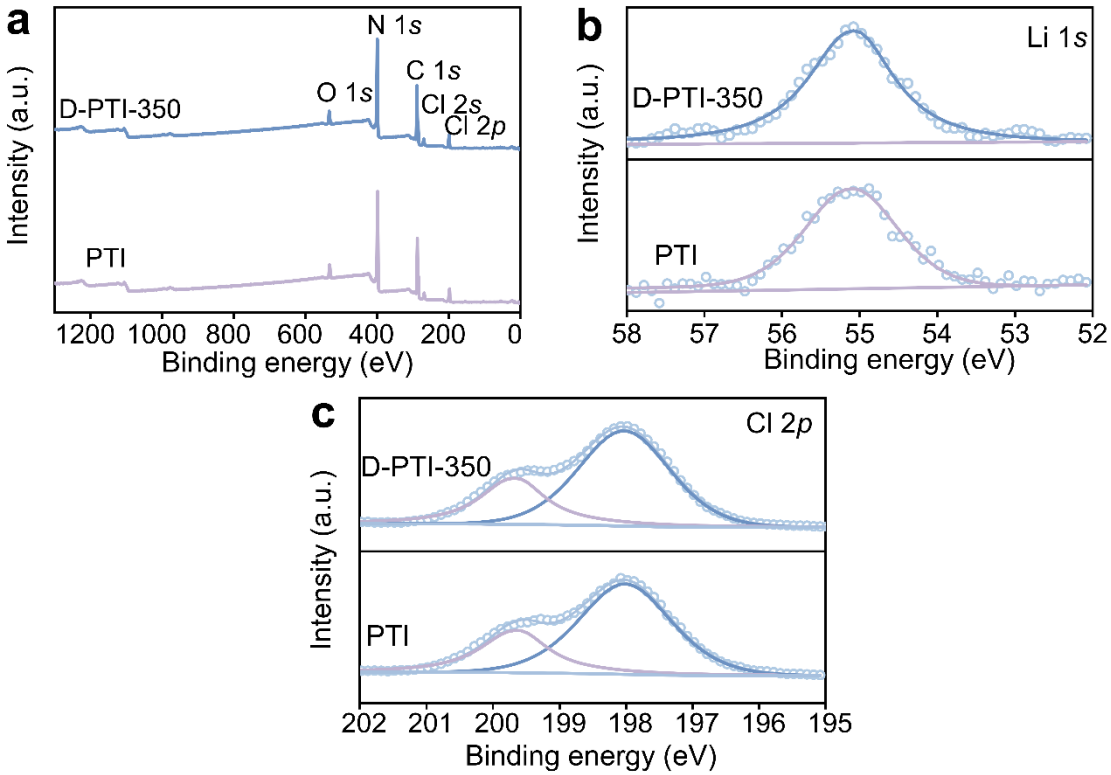

Fig. S6. (a) Survey XPS spectra, (b) Li 1*s*, and (c) Cl 2*p* XPS high-resolution spectra of as-prepared PTI and D-PTI-350.

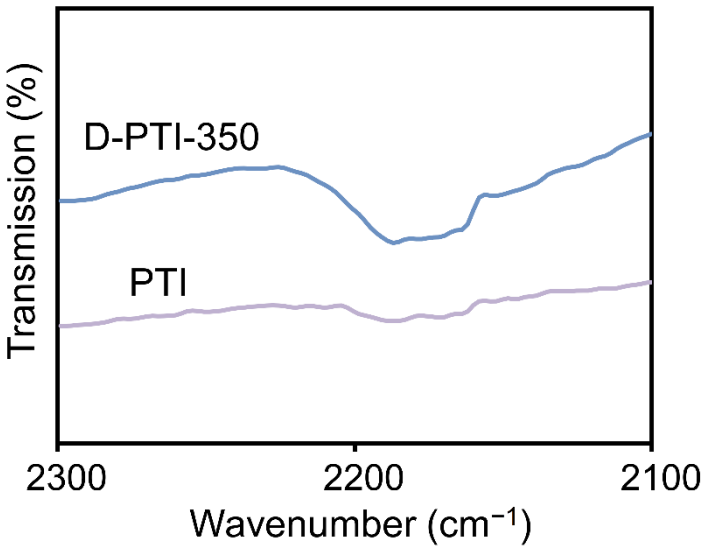

Fig. S7. Enlarged FT-IR spectra of PTI and D-PTI-350.

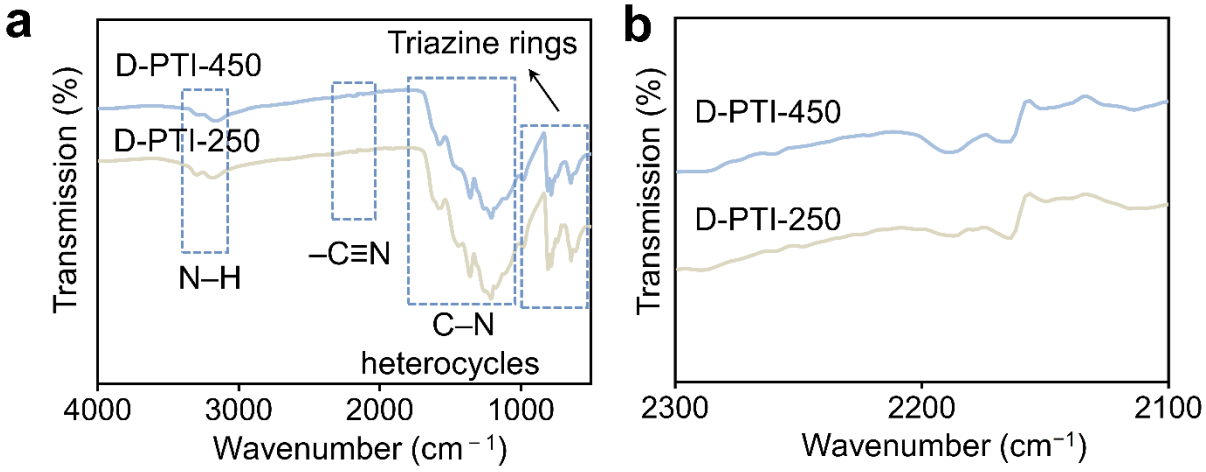

Fig. S8. (a) FT-IR spectra and (b) Enlarged FT-IR spectra of D-PTI-250 and D-PTI-450, respectively.

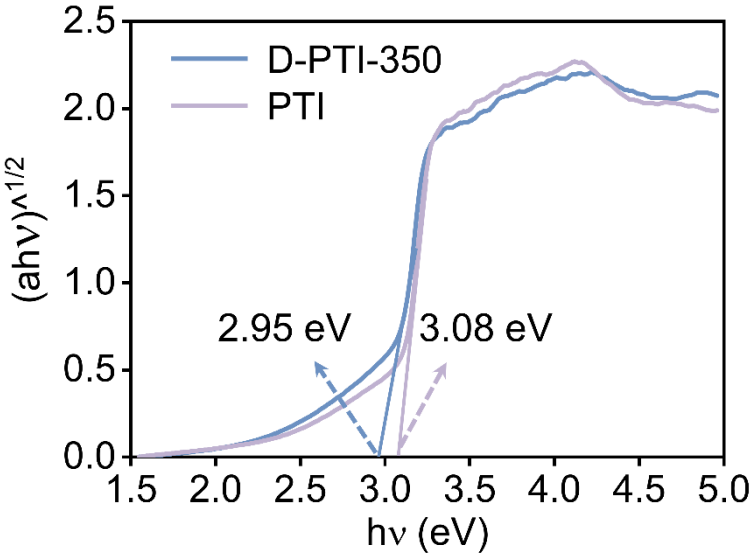

Fig. S9. Bandgap of PTI and D-PTI-350 determined by Tauc plots.

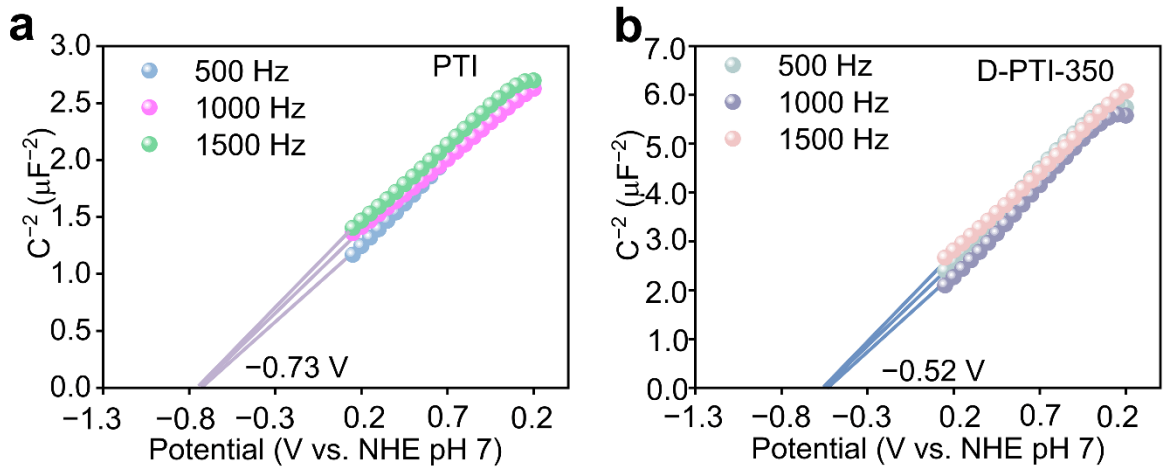

Fig. S10. The Mott-Schottky plots of (a) PTI and (b) D-PTI-350.

The flat band potentials of PTI and D-PTI-350 were determined by the Mott–Schottky (M–S) equation:[1, 3]

$$\frac{1}{C_{SC}^2} = \frac{2}{\varepsilon_r \varepsilon_0 A^2 N}\left(E - E_{fb} - \frac{kT}{e}\right)$$

where ε_r is the relative dielectric constant of the semiconductor, ε_0 is the vacuum dielectric constant, e is the elementary charge, A is the surface area, N is the free carrier density, k is the Boltzmann constant, T is the temperature, E is the applied potential and E_{fb} is the flat band potential.[4] By taking the x-intercept of a linear fit to the Mott–Schottky plot ($E_{fb} = E - \frac{kT}{e} \approx E$), the flat band potential of PTI and D-PTI could be estimated as −0.73 and −0.52 V (vs. NHE, pH 7). Because the conduction band value of the semiconductor is approximate to the flat band potential,[5] we could further obtain the conduction band minimum (E_{CBM}) of PTI and D-PTI-350 as −0.73 and −0.52 V (vs. NHE, pH 7).

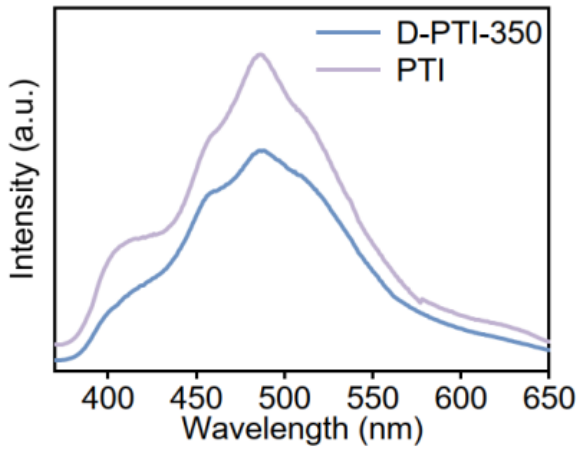

Fig. S11. Room-temperature PL spectra of PTI and D-PTI-350.

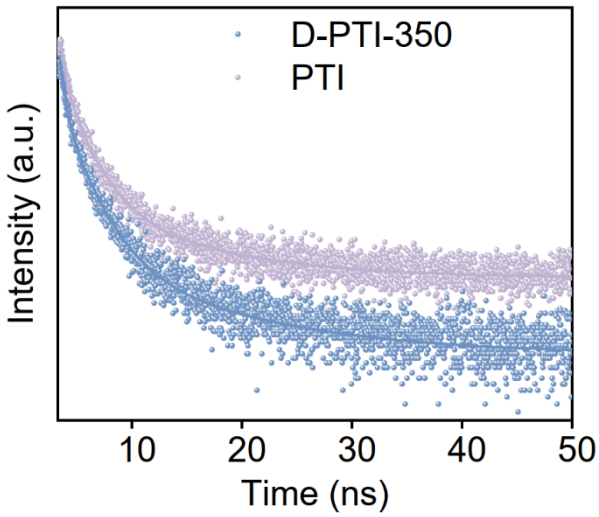

Fig. S12. Time-resolved PL spectra of PTI and D-PTI-350.

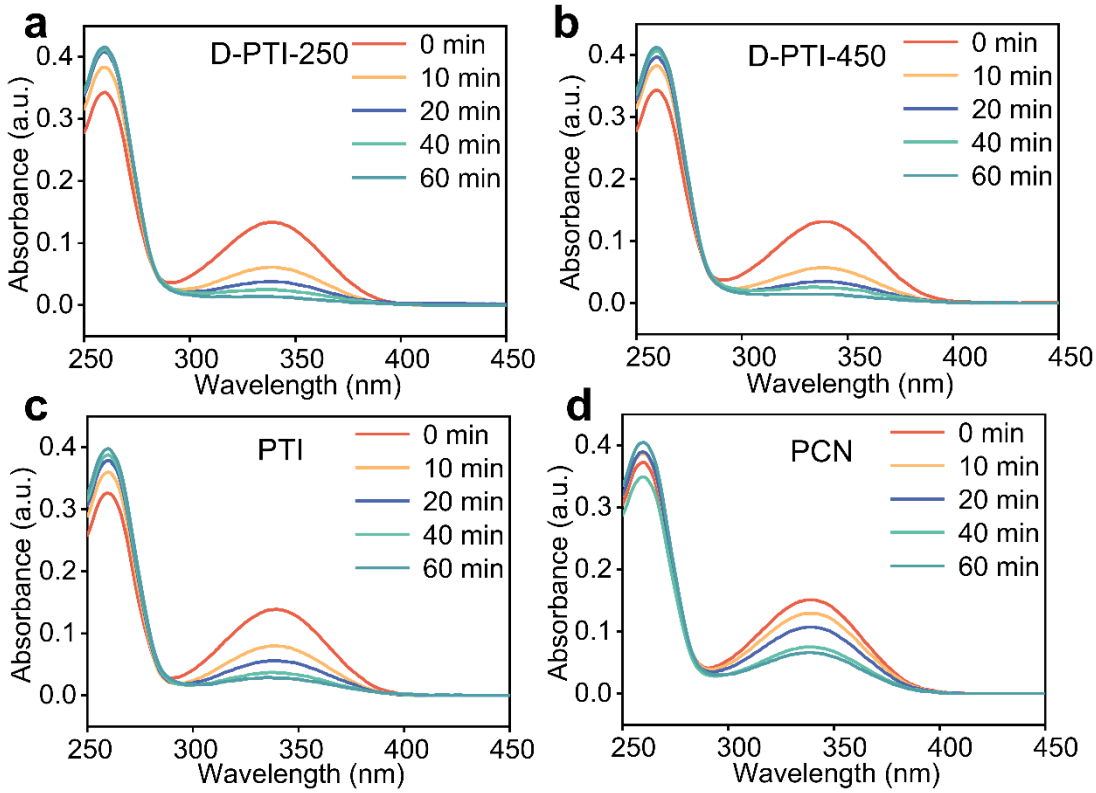

Fig. S13. UV–vis absorbance profile of NAD^+ regeneration over (a) D-PTI-250, (b) D-PTI-450, (c) PTI, and (d) PCN, respectively.

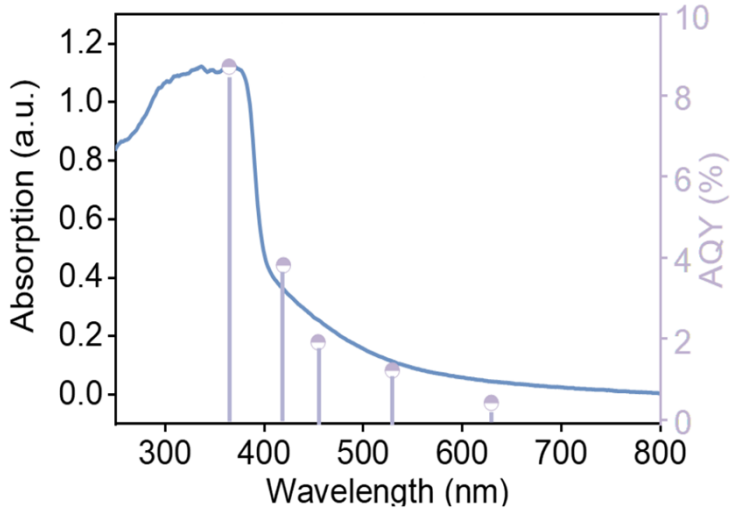

Fig. S14. Action spectra and wavelength-dependent apparent quantum efficiency over D-PTI-350.

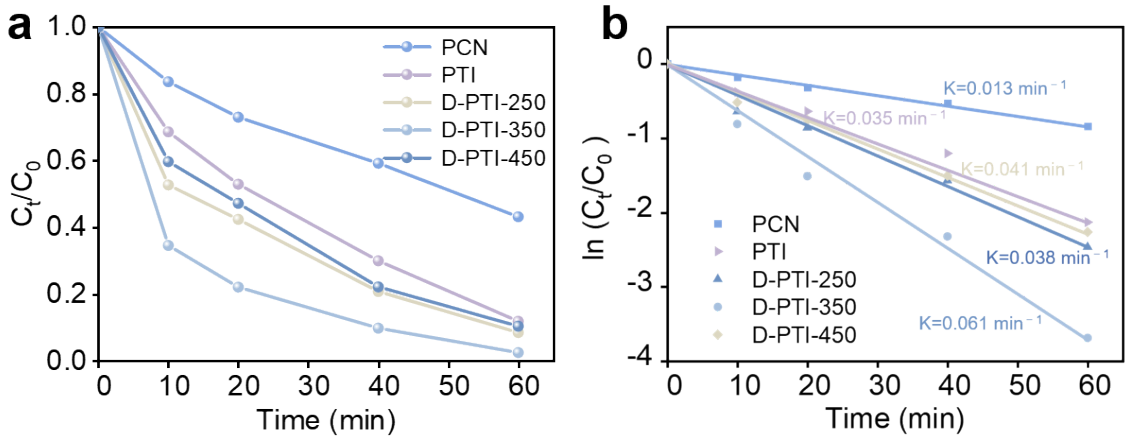

Fig. S15. (a) Photocatalytic activities for NADH oxidation over PCN, PTI, and D-PTI samples. (b) Rate constants of the catalytic oxidation reaction of NADH obtained with different catalysts through a plot of $\ln(C_t/C_0)$ versus time (T = 310 K).

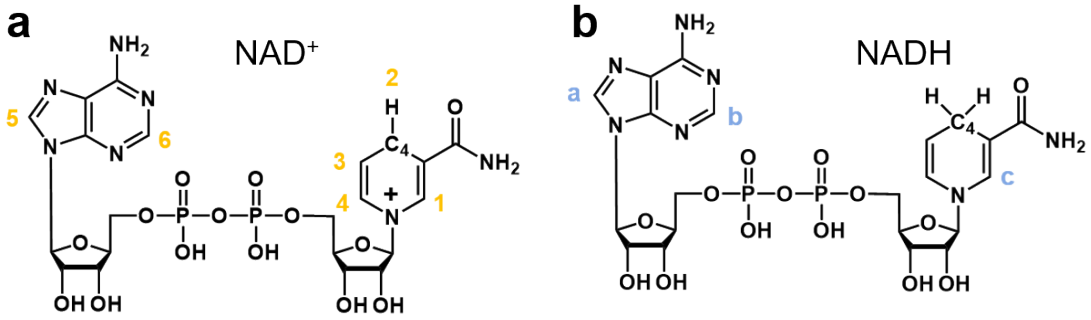

Fig. S16. The structure of (a) NAD^+ and (b) NADH.

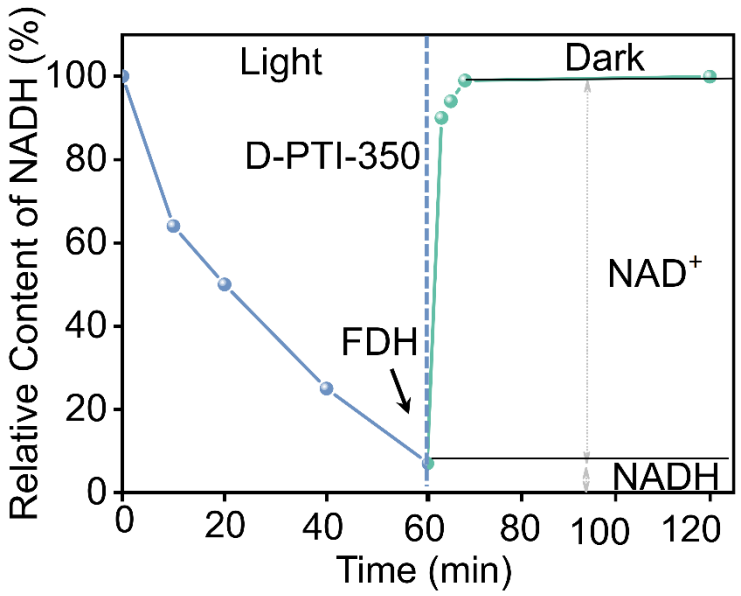

Fig. S17. Kinetic curve of NADH oxidation by D-PTI-350 and selective reduction of regenerated NAD^+ to 1,4-NADH by FDH after photocatalytic oxidation.

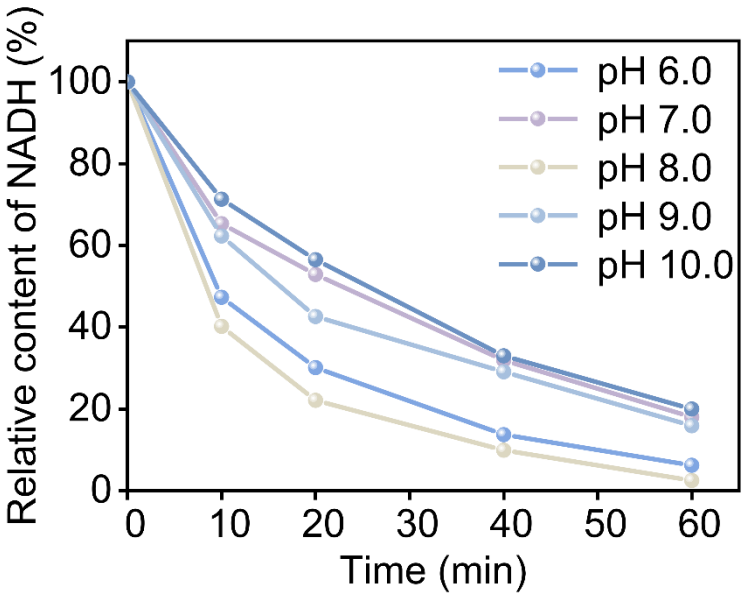

Fig. S18. Catalytic oxidation of NADH by D-PTI-350 at different pH.

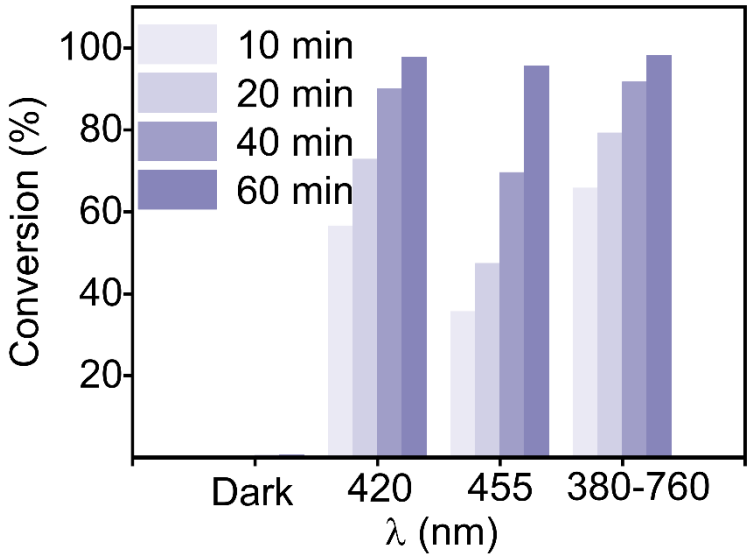

Fig. S19. Catalytic oxidation of NADH by D-PTI-350 at different wavelengths.

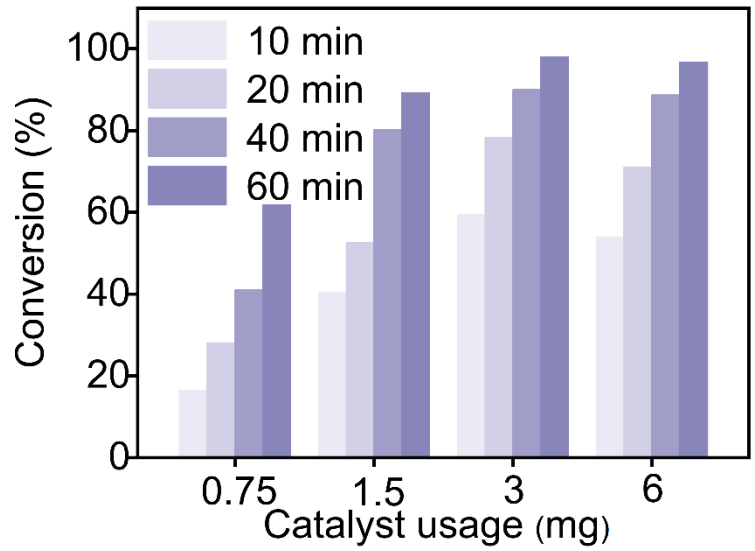

Fig. S20. Catalytic oxidation of NADH by D-PTI-350 at different catalyst usage.

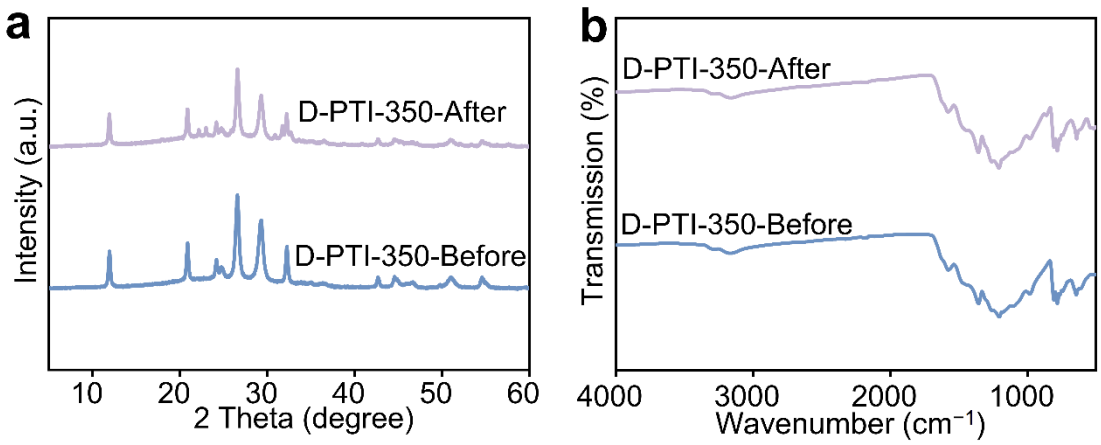

Fig. S21. (a) XRD and (b) FT-TR characterizations of D-PTI-350 before and after the reaction.

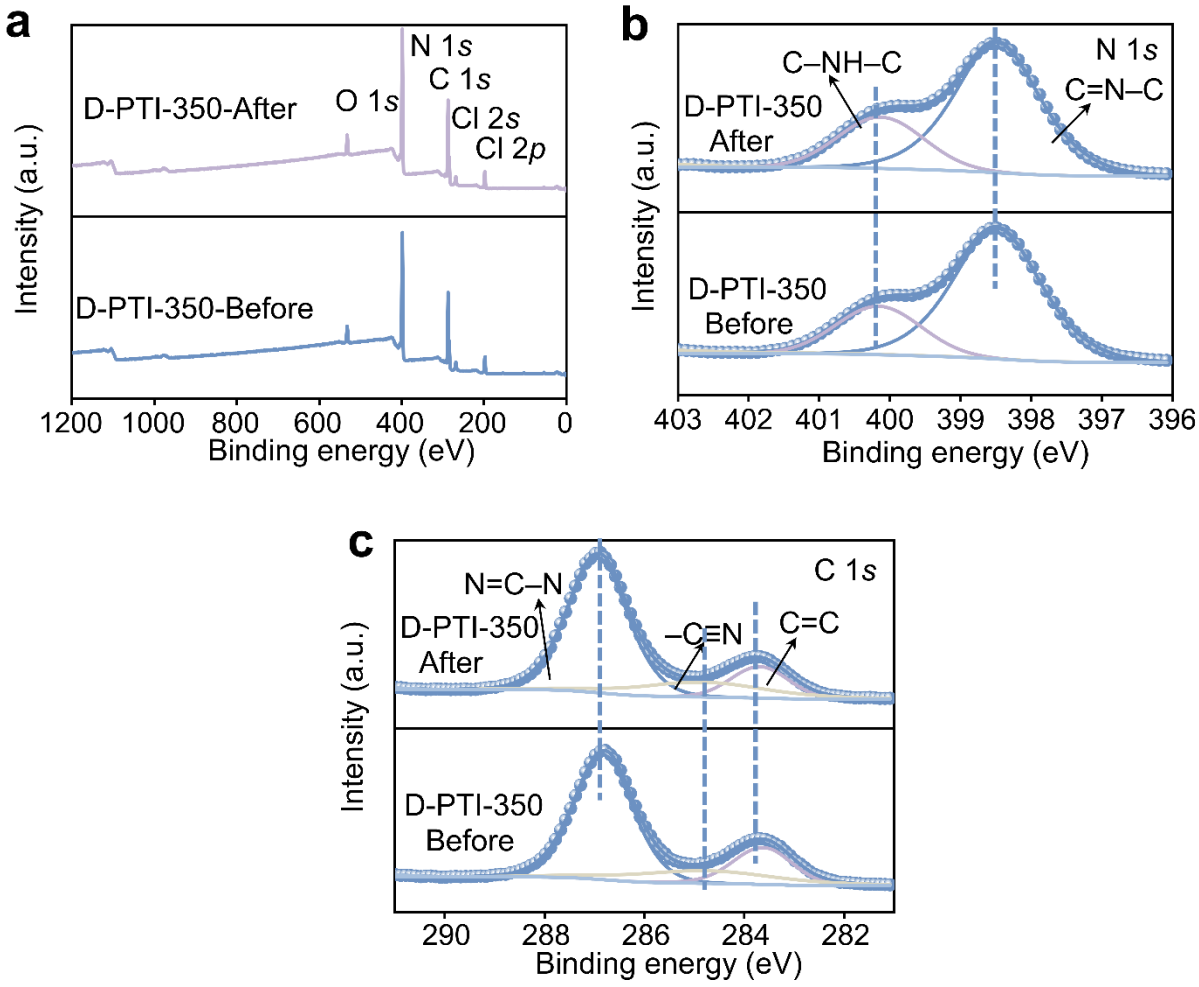

Fig. S22. (a) Survey XPS spectra, (b) Li 1*s* and (c) Cl 2*p* XPS high-resolution spectra of D-PTI-350 before and after the reaction.

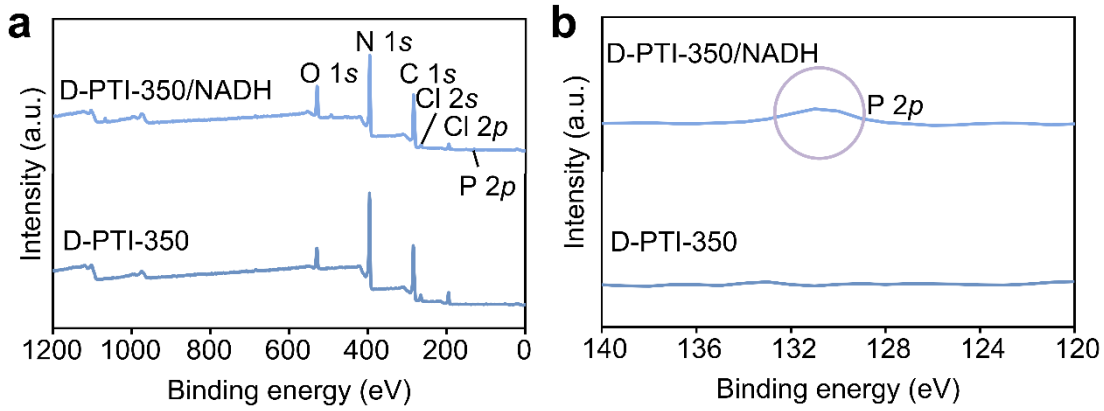

Fig. S23. (a) Survey XPS spectra and (b) P 2*p* spectra of D-PTI-350 after NADH adsorption.

Table S1. Comparative study on the oxidation performance of NADH by different photocatalysts.

Entry	Catalyst	Time [min]	Reactant solution	Light source [nm]	T [℃]	Con. [%]	Sel. [%]	Ref.
1	D-PTI	60	PBS, Air	380-700	37	98.2	99.9	This work
2	NP-CS	60	PBS, Air	>420	37	99.9	99.9	6
3	CdS	30	PBS, Air	>420	37	70.1	82.3	7
4	Vesicle	60	PBS, Air	380~700	37	99.9	99.9	8
5	Fe/CN	40	PBS, Air	>420	37	67.5	78.8	9
6	CMP-NPs	45	PBS, Air	420	37	75.0	99.9	10
7	B-BO_3	60	PBS, Air	>420	37	75.0	-	11
8	S-NC	30	PBS, Air	-	25	99.9	99.9	12
9	Cp*Ir-Complex	30	PBS, Air	-	25	96.0	99.9	13
10	CdS-140	120	PBS, Air	380~700	37	99.9	-	14
11	CuAsp	10	PBS, H_2O_2	-	25	85.0	20.0	15
12	N-CNTs	30	PBS, Air	-	25	60.0	80.0	16
13	NanoNOx	90	PBS, Air	-	25	99.9	99.9	17

Table S2. The element content in different chemical environments derived from XPS results.

Sample	N=C–N (%)	C=C (%)	–C≡N (%)	C=N–C (%)	C–NH–C (%)
PTI	67.59	32.41	-	47.48	52.52
D-PTI-350	66.91	21.77	11.32	44.79	55.21

Table S3. Fitting parameters for the time-resolved PL spectra of PTI and D-PTI-350.

Sample	τ_1	τ_2	τ_3	τ_{ave}	Goodness of fit
PTI	0.522 (7.43%)	2.369 (48.42%)	10.20 (44.36%)	8.54	1.029
D-PTI-350	0.516 (10.00%)	2.618 (50.04%)	12.34 (39.95%)	11.03	1.037

References

1. Arthur, J., Nozik, Rüdiger and Memming, *J. Phys. Chem. B*, 1996, **100**, 13061-13078.
2. Z. Zhang, W. Liu, Y. Zhang, J. Bai and J. Liu, *ACS Catal.*, 2020, **11**, 313-322.
3. K. Gelderman, L. Lee and S. Donne, *J. Chem. Educ.*, 2007, **84**, 685.
4. T. Han, X. Cao, K. Sun, Q. Peng, C. Ye, A. Huang, W.-C. Cheong, Z. Chen, R. Lin, D. Zhao, X. Tan, Z. Zhuang, C. Chen, D. Wang and Y. Li, *Nat. Commun.*, 2021, **12**, 4952.
5. S. J. Hong, S. Lee, J. S. Jang and J. S. Lee, *Energy Environ. Sci.*, 2011, **4**, 1781-1787.
6. W. Wei, F. Mazzotta, I. Lieberwirth, K. Landfester, C. T. J. Ferguson and K. A. I. Zhang, *J. Am. Chem. Soc.*, 2022, **144**, 7320-7326.
7. S. Zhang, J. Shi, Y. Chen, Q. Huo, W. Li, Y. Wu, Y. Sun, Y. Zhang, X. Wang and Z. Jiang, *ACS Catal.*, 2020, **10**, 4967-4972.
8. N. Zhang, S. Trepout, H. Chen and M. H. Li, *J. Am. Chem. Soc.*, 2023, **145**, 288-299.
9. Y. Zhang, X. Huang, J. Li, G. Lin, W. Liu, Z. Chen and J. Liu, *Chem. Res. Chin. Univ.*, 2020, **36**, 1076-1082.
10. S.-M. Jo, K. A. I. Zhang, F. R. Wurm and K. Landfester, *ACS Appl. Mat. Interfaces* 2020, **12**, 25625-25632.
11. B. C. Ma, L. Caire da Silva, S. M. Jo, F. R. Wurm, M. B. Bannwarth, K. A. I. Zhang, K. Sundmacher and K. Landfester, *Chembiochem*, 2019, **20**, 2593-2596.
12. D. Zhu, M. Zhang, C. Wang, P. Gai and F. Li, *Chem. Mater.*, 2022, **34**, 11072-11080.
13. Y. Maenaka, T. Suenobu and S. Fukuzumi, *J. Am. Chem. Soc*, 2011, **134**, 367-374.
14. H. Wang, J. Chen, Q. Dong, X. Jia, D. Li, J. Wang and E. Wang, *Nano Res.*, 2022, **15**, 5256-5261.
15. S. Liu, X. Wu, J. Xiong, X. Yuan, M. H. Zong and W. Y. Lou, *Mater. Chem. Front.*, 2022, **6**, 3391-3401.
16. H. Wang, J. Chen, Q. Dong, X. Sun, Q. Liu, D. Li, E. Wang and J. Wang, *Nano Res.*, 2023, **16**, 6615-6621.
17. A. Rodrigue-Abetxuko, A. Reifs, D. Sánchez-deAlcázar and A. Beloqui, *Angew. Chem. Int. Ed.*, 2022, **134,** e202206926.